Technical Paper

ISSN 1997-1400 Int. J. Pavement Res. Technol. 4(6):356-364

A New Method to Characterize the Stone-Stone Contact Degree of Asphalt Mixture Using X-ray Computed Tomography Images

Yuehua Duan[1+, 2], Xiaoning Zhang[1], Zhi Li[1], and Duanyi Wang[1]

Abstract: Until now, voids in the Coarse Aggregate (VCA) parameter were used to judge whether the coarse aggregate skeleton is formed in asphalt mixtures. However, this method has several shortcomings and deficiencies. In this paper, the X-ray Computed Tomography (CT) is used to obtain two-dimensional (2D) images through a series of digital image processing methods to separate the aggregates successfully. A contact searching method was established to find all the contacting pixels surrounding each particle. All pixels found were stored and analyzed. The contact degree changes, along with the different depths of the specimen, and the contacting pixel values calculated by the algorithm concentrate to approximately 0-20 pixels, which equals about 0-2 mm. Three quantitative indicators, *C*1, *C*2, and *C*3, were established. Their input data were fitted by 4 different probability density functions (PDFs): Normal distribution, Lognormal distribution, Gamma distribution, and Weibull distribution. The goodness of the fit was simultaneously tested through two different formal statistical tests (Kolmogorov-Smirnov and Chi-square) to provide mathematical support. Finally, the Lognormal PDF was found to be the most suitable for describing the input data distributions, and C1 was recommended as the quantitative indicator for the assessment of stone-stone contact degree.

Key words: *Asphalt mixture; Contact; Digital image processing; VCA; X-ray computed tomography.*

Introduction

Rutting is one of the major causes of damage to asphalt pavement. Many local and foreign road researchers have carried out numerous studies concerning the rutting of asphalt pavement. Different types of modified asphalt have been adopted to improve the road performance of asphalt mixture. In addition, different types of pavement structure design methods have been invented and put into practice successfully, such as Stone Matrix Asphalt (SMA) and Coarse Aggregate Void Filling method (CAVF) [1].The key point of these methods lies in the formation of the coarse aggregate skeleton.

All of these methods have a very important parameter— voids in the Coarse Aggregate (VCA). The voids in the Coarse Aggregate of Asphalt Mixture (VCA_{mix}) is defined as below:

$$VCA_{mix} = \left(1 - \frac{\gamma_f}{\gamma_{ca}} \times P_{ca}\right) \times 100 \quad (1)$$

where：

P_{ca}= the proportion of particles (%) that is greater than 4.75 mm.

γ_f = the bulk relative density of asphalt mixture specimen.

γ_{ca} = the average bulk relative density of the coarse aggregate skeleton.

The voids in Coarse Aggregate Under Tamping State (VCA_{drc}) is defined as Eq. (2):

$$VCA_{drc} = \left(1 - \frac{\gamma_f}{\gamma_{ca}}\right) \times 100 \quad (2)$$

where:

γ_s = the tamping bulk relative density.

And Eq. (3) was used to judge whether the skeleton of coarse aggregate is formed:

$$VCA_{mix} \le VCA_{drc} \quad (3)$$

From Eqs. (1) and (2), it can be seen that the volume parameters are calculated by bulk relative density. In other words, one cannot acquire the volume parameters directly. However, the whole experiment and calculation process do not specifically take the absorption of asphalt by aggregates voids into consideration, inevitably resulting in deviations [2].. Although the result is not very reliable, Eq. (3) is currently the only accepted formula to judge whether the stone-stone skeleton is formed.

Using X-ray Computed Tomography (CT), one can obtain the internal microstructure of asphalt mixture from the two-dimensional (2D) images, which have rich details. Many scholars have completed important academic work using this non-destructive method [3-12]. However, for this research on the coarse aggregates of asphalt mixture, the emphasis rests on the internal particles morphology. Garboczi [13] describes a mathematical procedure using spherical harmonic functions to characterize the concrete aggregate particles and other particles of the same nature. Erdogan *et al.* [14] compares shape data on several different kinds of coarse aggregates and illustrates potential mathematical shape analyses made possible by spherical harmonic information. Taylor *et al.* [15] discusses some of the properties of irregular particles, including volume, density and surface areas, while studying the rocks' shapes by combining three dimensions with their volumes and surface areas. Wang *et al.* [16] reconstructed a three-dimensional digital

[1] School of Civil Engineering and Transportation, South China University of Technology, Guangzhou, China 510640;

[2] Guangdong Hualu Communications Technology Co., Ltd., Guangzhou, China 510420.

[+] Corresponding Author: E-mail dyh_scut@yahoo.com.cn

Note: Submitted August 29, 2010; Revised March 24, 2011; Accepted March 29, 2011.

Table 1. Aggregate Gradation

Aggregate Gradation	Cumulative Percent Passing by Weight (Square Openings, mm)									
	16	13.2	9.5	4.75	2.36	1.18	0.6	0.3	0.15	0.075
AC-13	100	95	70	48	36	24	18	12	8	4

Note: AC-13 is from *Specifications of Asphalt Concrete Pavement Design for Highway* used in China and represents specific aggregate gradation type, among which the last number stands for the nominal maximum aggregate size of asphalt mixtures.

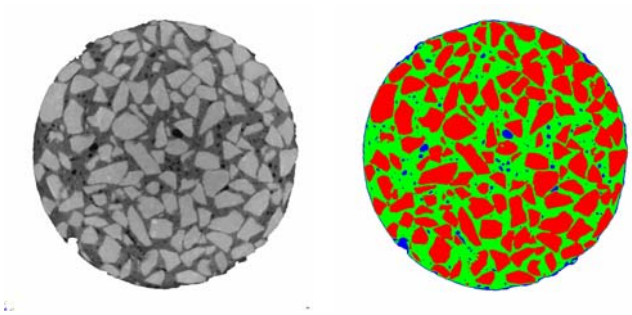

(a) Original Image (b) After Segmentation

Fig. 1. Segmentation Result Map

representation of individual particles in a granular system and presented the quantities needed for subsequent simulation of particle behavior, including the volume and the momentum of inertia of each particle. Masad *et al*. [17] put forward that the X-ray CT images, in conjunction with spherical harmonic analysis, were a powerful technique in representing and reconstructing three-dimensional images of particles, which can be used to mathematically represent the shape of particles in computational models. However, there has yet been no special research on the aggregates' contact status from published research results.

Using X-ray CT images, the positional relationship from particle to particle in asphalt mixtures can be easily observed. In this paper, digital image processing methods were adopted to deal with the 2D images obtained by X-ray CT with each 2D image divided into four components: background, pores, mastics and aggregates. Then the adhesion particles were separated by a specific digital image processing method. After that, the contact search method was used to find all the contacting pixels surrounding each single particle. All contacting pixels found were recorded and then analyzed carefully from different angels. Finally, three quantitative indicators were tried to be established, and their input data were tested by the fitting process. Finally, the most appropriate one was recommended

Objectives

The objectives of this study are 1.) to find a suitable method that can reveal the inherent laws of aggregate contact status in asphalt mixture based on digital image processing methods using X-ray CT images and 2.) to establish a quantitative indicator to characterize the stone-stone contact degree.

Asphalt Mixtures Specimen Preparation and Scanning

In this research, the granite is used as aggregate particles and Shell #70 petroleum asphalt as binder. Meanwhile, AC-13 was selected as the asphalt mixtures specimen. Table 1 gives the aggregates' gradation. With the optimum asphalt content, the corresponding cylindrical specimen was compacted by the Marshall compactor in the laboratory.

The 225 kV industrial CT assembled by YXLON Company was used to acquire the scanning images, and the VGStudio MAX 2.0 software was used to realize the three-dimensional (3D) visualization. After the 3D reconstruction process, a total of 640 2D slice images were received, and the resolution in the X-Y plane and along the Z axis are the same 0.10 mm/pixel.

Digital Image Processing

Segmentation Process

To acquire good segmentation effect on these 2D images, some original image pre-processing work must be done. CT scan images are pseudo-color and should first be transformed into gray scale. The original images contain a lot of noise, so the adaptive Gaussian filter was selected to deal with the original images. The morphological open operation was implemented to remove the bright details smaller than the structural element while completely deleting target regions that cannot contain the structural element, smoothing contours of the objects, disconnecting the narrow connection, removing the small prominent parts, and finally filling tiny holes within aggregates. All procedures above were executed using MATLAB.

The Maximum Classes Square Error Method (OTSU method) was proposed by Japanese scholar Otsu, and it is a self adaptive threshold determining method [18].

Suppose a gray image's total average gray value can be expressed as Eq. (4):

$$u = w_0 \times u_0 + w_1 \times u_1 \tag{4}$$

where:
u = the image's total average gray value.
w_0= the foreground proportion (%).
u_0= the foreground average gray value.
w_1= the background proportion (%).
u_1= the background average gray value.

The classes' square error g can be expressed as Eq. (5):

$$g = w_0 \times (u_0 - u)^2 + w_1 \times (u_1 - u)^2 \tag{5}$$

Suppose t is the foreground and background segmentation threshold gray value, then the t, value, which makes the g achieve the greatest value, is the optimal segmentation value.

Here, the two classification strategy was used twice based on the OTSU method to separate each 2D slice image into four different components: background, aggregates, mastics, and voids. Fig. 1

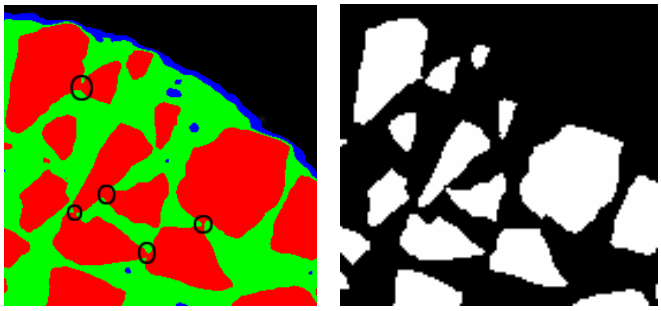

(a) Before Processing (b) After Processing

Fig. 2. Adhesion Treatment Results Map

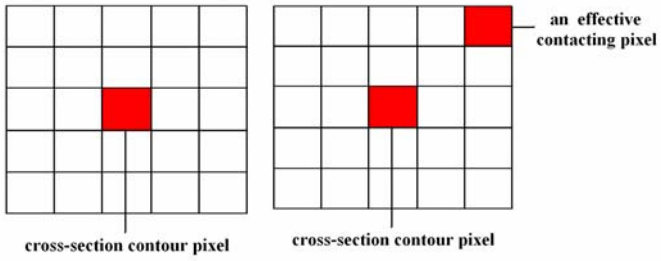

(a) No Contacting Pixel (b) One Contacting Pixel

Fig. 3. Contact Searching Diagram

shows the final segmentation result.

Adhesion Problem

After careful observations of Fig. 1(b), the aggregates were found to be not totally separated into single particle as completely as what can be seen in Fig. 2(a). The black circles indicate an adhesion problem. The reasons are complex. Generally speaking, it is affected by the original 2D images' quality.

The adhesion point bonds different particles together, making it impossible to be analyzed as a single entity. Previous researchers frequently used Photoshop, Image-Pro (software name), etc. to separate the cohering pixels.

The digital image processing method was designed to deal with this problem. There will be similar adhesion problems in the complex cytological and histological images since the cells may overlap and cluster strongly, making the segmented structures deviate from the final quantification of features of single cells. Scholars [19] have put forward an algorithm named the Morphological Multiscale Decomposition (MSD) by which the cells are separated from each other successfully. Here, the main idea of the pseudo-code was cited, and according to the asphalt mixtures' 2D image features, the code was adjusted and then executed by MATLAB. Fig. 2(b) is the final result map. From the image, it can be seen that the particles sticking together are completely separated one by one.

Judgment of Stone-Stone Contact and Fundamental Contact Status Analysis

It is the asphalt film thickness concept that should be first considered in this research. If the aggregate particles are fully in contact with each other, the edges should be very close. Elseifi *et al.* used the Scanning Electron Microscopy (SEM) to observe the microstructure of asphalt mixtures, showing that asphalt binder films surrounding large aggregates actually consist of asphalt mastic films. These mastic films are highly irregular in shape and have a thickness of greater than 100 μm of the considered mixture [20]. According to this conclusion, if two adjacent aggregates are fully in contact, the particles boundary interval can be defined as no more than 2 pixels being consistent with the actual resolution of the images.

Contact Searching Method Design

Design a 5x5 square window and take the particles boundaries as a search path to carry out a complete perimeter search with the pixel point representing the aggregate boundary, which is always located in the center of the window. During the search process, if other pixels are found in the window, the stone-stone contact was deemed to occur, and the pixels will be recorded. Meanwhile, the following constraint conditions should be determined. Any pixel found in the square window that belongs to the particle itself should not be misjudged as an effective contacting pixel. During the search process, any repeated pixels found when the square window moves along the boundary of single particle should not be recorded repeatedly. All contacting pixel data were stored in the cell unit form by MATLAB. The contact search diagram can be seen in Fig. 3.

Since the slice image's resolution was very high, the X-Y plane and the Z axis pixel are all 0.10mm/pixel, making the spacing between two adjacent layers very small (about 0.10 mm). It can be deduced that any effective particle-to-particle contact will be reflected in the two-dimensional slice images.

According to the methods mentioned above, the total of 640 2D images obtained by X-Ray CT implemented the search process sequentially from top to bottom. The basic configuration for the computer is as follows: Pentium Dual-Core CPU 2.5 GHz, 2 GB memory, and 512 MB Graphics Memory. The average processing time for a single slice image was about 3.5-5 minutes, and the total time needed was about 40 hours. Since the search and storing process was limited by the ordinary computer's memory capacity, the time consumed was a bit too long. However, the efficiency would improve greatly by using a more advanced computer.

Data collection and Fundamental Analysis of Contact State

The raw data collected for this research include every aggregate perimeter, area, total number of particles, total contacting points and their corresponding pixels found in each 2D image.

Through the above search process, a total of 16,984 effective contact points were found in the 640 2D images with the minimum value of a single point's contact searching pixel being 1, which corresponds to 0.1 mm. The maximum value of a single point's contact searching pixel is 145, which corresponds to an actual size 14.5 mm. The maximum value fits the maximum size of aggregates of AC-13 asphalt mixture very well, proving the validity of the contact searching process indirectly.

How the amount of effective contact points changed along the 2D

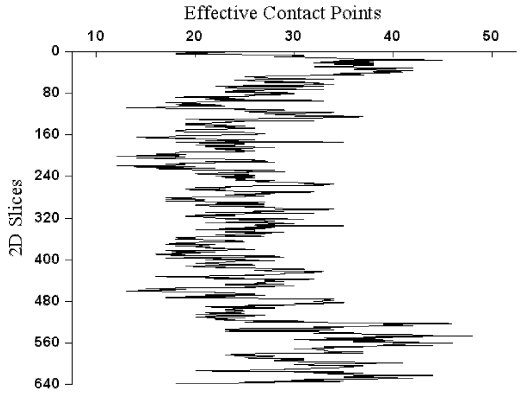

(a) Effective Contact Points

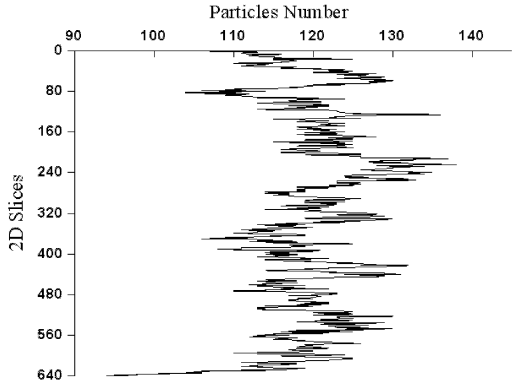

(b) Particles Number Distribution

Fig. 4. Effective Contacting Points and Particles Number Variation Rule

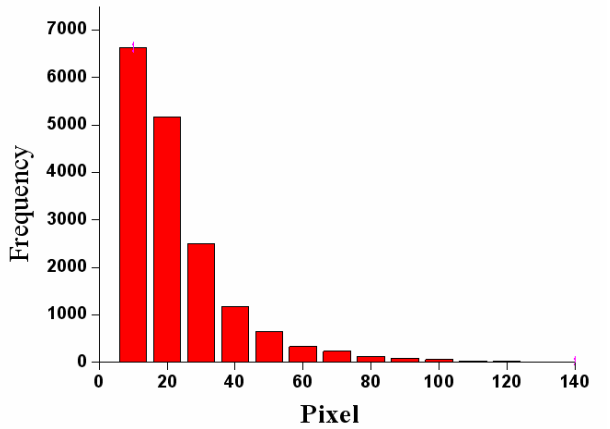

Fig. 5. Contacting Pixels Frequency Histogram.

sections can be seen in Fig. 4(a). There are more effective contacting points at the top 6.5 mm and at the bottom 11 mm than at the middle part of the specimen. It can be deduced that since the top part is under the drop hammer and the bottom part is directly in contact with the steel pad, it would be more effective if contact points were searched out by the algorithm. However, from Fig. 4(b), the particle amount in each slice image along the 2D sections has no clear rule at all.

All the pixel values corresponding to each contact point found in the 640 sections were put together, and then the frequency histogram was drawn at the interval of 10 pixels (Fig. 5).

Fig. 5 shows that the pixel distribution basically concentrates around the range of 0-20 pixels (the actual length should be 0-2 mm) with a cumulative distribution frequency of 69.5%. The figure explains that most contact points in this AC-13 asphalt mixture with floating and compact structure are point contact, which shows a small value of contacting pixels. It can be deduced that if the aggregate has a very regular particle shape and the coarse aggregate skeleton forms very well, there should be more surface contact reflecting the general improvement of contact pixel value in 2D slice images. This means the pixel distribution should have a very different form than what we see in Fig. 5.

Stone-Stone Contact Degree Quantitative Indicator

In order to quantify the contact degree of aggregates, there wouldn't be much practical value in only making statistics of contact pixels, but one can give an objective assessment on the contact degree by combining the particle distribution and geometry. Here, we collect the total amount of particles, total amount of pixels on behalf of the aggregates' perimeter, and total amount of pixels on behalf of the aggregates' area in each 2D slice image. Then, we compare the different above values to the contact pixels in the same 2D image to determine the equations of contact degree as follows:

$$C1 = \frac{N_{pixels}}{G_{total}} \tag{6}$$

$$C2 = \frac{N_{pixels}}{C_{total}} \tag{7}$$

$$C3 = \frac{N_{pixels}}{A_{total}} \tag{8}$$

where:

N_{pixels}= the total amount of contact pixels in each slice image.

G_{total}= the total amount of particles in the same slice image.

C_{total} = the total amount of pixels on behalf of aggregates' perimeter in the same slice image.

A_{total} = the total amount of pixels on behalf of aggregates' area in the same slice image.

As can be seen from Fig. 6, $C1$, $C2$, and $C3$ have similar variation rules along the 2D slice top to bottom just like the effective contact points in Fig. 4(a).

Fitting Distributions of Quantitative Indicator

This paper selected several probability distributions to analyze the indicators. Probability distributions have been used by numerous researchers in the modeling of construction activities. Generally, there are two ways to achieve this [21]. They include a.) using the collected data to define an empirical distribution and b) fitting a theoretical distribution to the collected data. We chose the latter manner. The steps to fit theoretical probability distributions to the input data are:

1. Create input data histogram;
2. Select probability distribution functions;

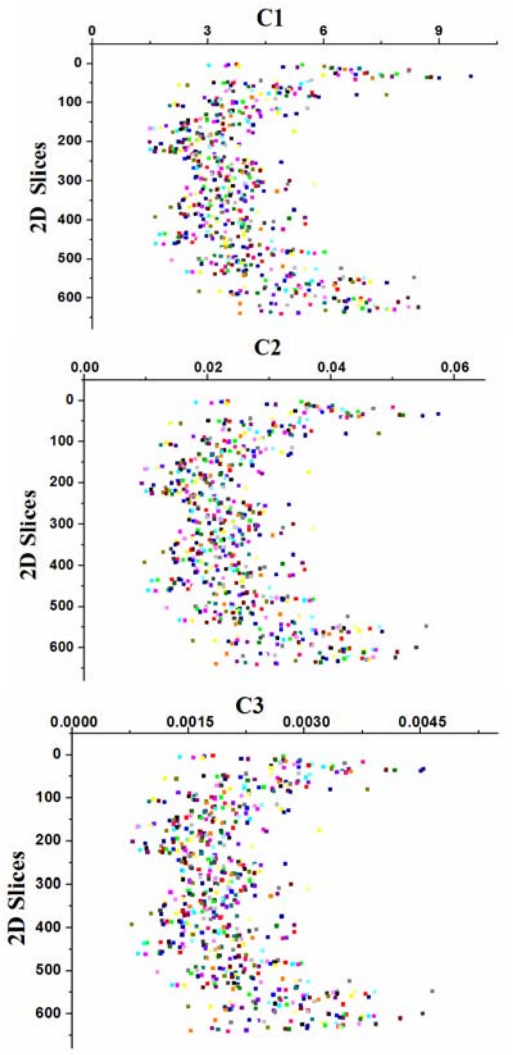

Fig. 6. *C*1, *C*2, and *C*3 Variation Rule

3. Fit different distribution functions to the input data;
4. Assess the goodness of fit.

Creating Input Data Histogram

Histograms are applicable to continuous distribution and provide a readily interpreted visual synopsis of the collected data. However, there is debate regarding how many intervals are the most scientific. Much research has been done on applying class interval rules, and numerous views were proposed [21]. Montgomery and Runger [22] put forward that intervals should be used in order to avoid uninformative histograms between 5 to 20. Kottegoda and Rosso [23] set a lower and upper bound for class interval quantity of 5 to 20, respectively. Neville and Kennedy [24] regarded 10 and 25 as the lower and upper bounds, respectively. Law and Kelton [25] proposed that a number of histograms should be produced according to a number of different intervals, and the one that has the smoothest shape should be selected. The authors compared the 8, 10, 12, and 14 class intervals.

Here, the range of contacting pixel values was broken up into 10 disjointed intervals, with all intervals having the same width Δ. Taking the *C*1 values, for example, the minimum value of *C*1 is 1.33, and the maximum value of *C*1 is 9.81, so the interval is 0.85. For j=1, 2,…,10, let h_j be the portion of x_i that are in the jth interval, so the function is defined as Eq. (9):

$$h_x = h_j, \text{ if } C1_{\min} + (j-1)*\Delta \le x < C1_{\min} + j*\Delta \quad \text{for } j = 1, 2, \ldots, 10 \tag{9}$$

where:
x = the *C*1 value.

It is plotted as a function of *C*1, and the plot of h was a piecewise constant just like Fig. 7.

Selecting Probability Distribution Functions (PDFs)

According to the histogram shape in Fig. 7, there are four different probability distribution functions (PDF): Normal distribution, Lognormal distribution, Gamma distribution and Weibull distribution. These 4 PDFs were selected to fit the raw data of C1, C2, and C3 simultaneously. The PDF of 4 different distributions can be expressed as Eqs. (10)-(13):

$$\text{Normal PDF: } y = \frac{1}{c\sqrt{2\pi}} e^{\frac{-(x-b)^2}{2c^2}} \tag{10}$$

where b is the mathematic expectation, and c is the standard deviation.

$$\text{Lognormal PDF: } y = \frac{1}{xc\sqrt{2\pi}} e^{\frac{-(\ln x-b)^2}{2c^2}} \tag{11}$$

where b is the mean of random variable ln*(x)*, and c is the standard deviation of ln*(x)*.

$$\text{Gamma PDF: } y = \frac{b^c}{\Gamma(c)} x^{c-1} e^{(-bx)} \tag{12}$$

where Γ is the Gamma function, b is the scale parameter, and c is the shape parameter.

$$\text{Weibull PDF: } y = \frac{c}{b}\left(\frac{x}{b}\right)^{c-1} \exp\left[-\left(\frac{x}{b}\right)^{c}\right] \tag{13}$$

where b is the scale parameter, and c is the shape parameter.

Fitting different PDFs to the Input Data

The above 4 PDFs were fitted to the input data of *C*1, *C*2, and *C*3, and the maximum likelihood estimation method (MLE) was used to estimate parameter values of different PDFs. The likelihood function can be expressed as Eq. (14):

$$L(\theta) = f_\varsigma(X_1) f_\varsigma(X_2) .. f_\varsigma(X_n) \tag{14}$$

where the MLE is defined to be the value of θ that maximizes $L(\theta)$ over all permissible values of θ.

The PDF can be calculated after the parameter values are

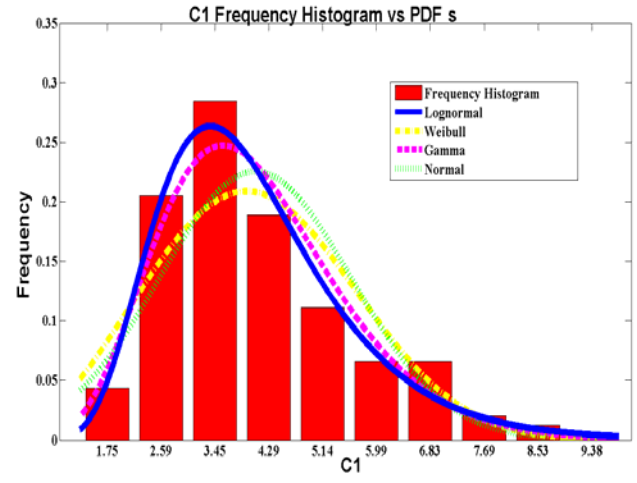

(a)

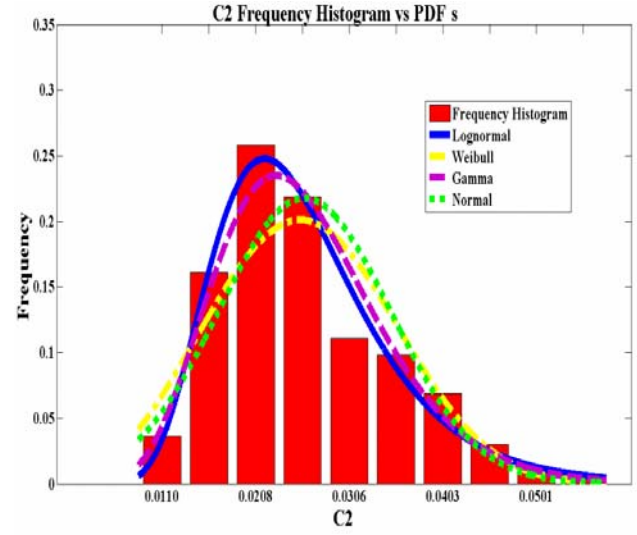

(b)

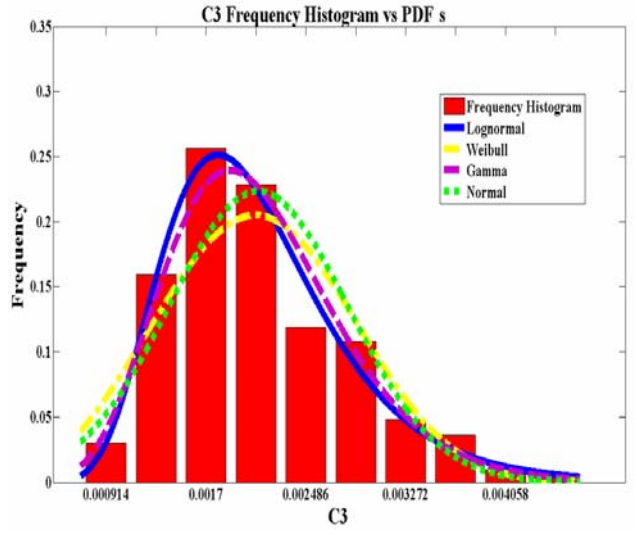

(c)

Fig. 7. Lognormal, Weibull, Gamma, and Normal Probability Density Functions for C1, C2, and C3.

estimated by MLE, and the PDF can be plotted as a function of x. The PDF curve can be placed on top of the plot of the input data histograms, as seen in Fig. 7.

Assessment of Goodness of Fit

Although a visual assessment of the goodness of fit through comparing the shape of the PDF with the shape of the histogram is often the superior method [26], it is always subject and prone to potential human error. Mathematical support for the assessment can greatly improve confidence in the goodness of fit. Here, the Kolmogorov-Smirnov test and the Chi-square test are utilized together for assessment.

The Kolmogorov-Smirnov test compares the distribution of x with the hypothesized continuous distribution [27]. The result value of h is 1 if the null hypothesis can be rejected at the 5% significance level, but the result value of h is 0 if the null hypothesis cannot be rejected at the 5% significance level.

The Chi-square test performs a goodness of fit test on the default null hypothesis that the data in vector x are a random sample from an arbitrary continuous distribution [28]. The result value of h is 1 if the null hypothesis can be rejected at the 5% significance level, but it will reduce to 0 if the null hypothesis cannot be rejected at the 5% significance level. Different from the Kolmogorov-Smirnov test, the Chi-square test is performed by grouping the data into bins, calculating the observed and expected counts for those bins, and computing the chi-square test statistics.

Data Analysis and Results

The aim of the data analysis is to find the most appropriate PDF that will best fit the input data of *C*1, *C*2, and *C*3. The plot of lognormal, Weibull, gamma, and normal distributions are shown in Fig. 7, demonstrating that the histograms all have 10 class intervals. From the figure, it can be seen easily that *C*1, *C*2, and *C*3 data histograms are all skewed to the right and have a right tail that swiftly falls in probability. The 4 PDFs all bear some resemblance to the underlying histograms, but they all over- or underestimate the histograms in different parts, which will reduce the accuracy of the analysis. It is difficult to determine which distribution is the best fit simply by visual assessment, making the formal statistical tests very important in providing mathematical support. The Kolmogorov-Smirnov test and Chi-square test results can be seen in Table 2.

From Table 2, we can see the lognormal distribution is the only PDF that passes all hypothesis tests at the 5% significance level when fitted to the input data of *C*1, *C*2, and *C*3. The p values for the Kolmogorov-Smirnov tests are 0.1772, 0.4549, and 0.8362, respectively. For *C*2, and *C*3, the Gamma distribution also passes the hypothesis test together with lognormal distribution at the 5% significance level, and the p values for the Kolmogorov-Smirnov tests are 0.0545 and 0.1499, respectively. The Chi-square test results are consistent with the Kolmogorov-Smirnov tests. The lognormal distribution passes all hypothesis tests at the 5% significance level, and the Gamma distribution passes the tests for *C*2 and *C*3 data. The respective p values for lognormal are 0.2916, 0.4990, and 0.4718, while for gamma they are 0.1882, and 0.0687. The Weibull and normal PDFs were ruled out for further consideration because they did not pass the hypothesis tests.

The statistical values of the Kolmogorov-Smirnov test were compared with those of the Chi-square test for the assessment of

Table 2. Parameter Estimations and Results for the Kolmogorov-Smirnov Test and Chi-square Test

Data	PDF	Parameter Values		Kolmogorov-Smirnov Test			Chi-square Test		
		b	C	h	p	Statistical Value	h	p	Statistical Value
*C*1	Lognormal	1.343	0.357	0	0.1772	0.0432	0	0.2916	47.581
	Weibull	4.586	2.863	1	0.0000	0.1024	1	0.0000	149.162
	Gamma	7.984	0.5115	1	0.0057	0.0674	1	0.0449	65.786
	Normal	4.084	1.501	1	0.0000	0.1137	1	0.0000	160.193
*C*2	Lognormal	-3.711	0.3412	0	0.4549	0.03361	0	0.4990	43.358
	Weibull	0.0289	3.0508	1	0.0000	0.09272	1	0.0000	113.172
	Gamma	8.816	0.0029	0	0.0545	0.05605	0	0.1882	57.549
	Normal	0.0259	0.0089	1	0.0000	0.1008	1	0.0000	113.288
*C*3	Lognormal	-6.213	0.329	0	0.8362	0.0243	0	0.4718	42.988
	Weibull	0.0024	3.16	1	0.0002	0.0839	1	0.0000	126.997
	Gamma	9.491	0.0002	0	0.1499	0.0447	0	0.0687	63.277
	Normal	0.0021	0.0007	1	0.0001	0.0879	1	0.0000	114.467

goodness of fit. For *C*1, the lognormal PDF is the only suitable distribution. For *C*2, the statistical value for lognormal PDF (0.03361) is smaller than the gamma PDF value (0.05605) where the Kolmogorov-Smirnov test is concerned. That is to say that with regard to the goodness of fit for *C*2, the lognormal PDF is better than the gamma PDF. For *C*3, the lognormal value (0.0243) is smaller than the gamma value (0.0447). The Chi-square test produces the same conclusions that the statistical values of lognormal PDF are smaller than those of gamma PDF for *C*2 and *C*3. Therefore, the lognormal distribution is considered the best PDF for describing the input data of *C*1, *C*2, and *C*3.

From the above analysis, it can be seen that the data of C1, C2, and C3 have very similar statistical distribution since they all fit the lognormal distribution very well.

From the expressions of *C*1, *C*2, and *C*3, it can be seen that *C*1 can be interpreted as the average amount of contact pixels of a single particle in each slice image. In comparison, *C*2 can be interpreted as the average amount of contact pixels per perimeter pixel unit of all particles in each slice image, and *C*3 can be interpreted as the average amount of contact pixels per area pixel unit of all particles in each slice image. It is clear that *C*1 is easier to understand and has a more explicit physical meaning than *C*2 and *C*3.

Moreover, in this example, the value of *C*1 varies from 1.33 to 9.81, the *C*2 value varies from 0.0086 to 0.0574, and the *C*3 value varies from 0.00072 to 0.00465, enabling the *C*1 raw data to be easier to record and to establish a statistical model.

In summary, *C*1 was recommended as the indicator reflecting the stone-stone contact degree of asphalt mixture specimen within a meso-scale.

The *b* and *c* of lognormal PDF are the most important parameters, with *b* being the mean of ln(*x*), and *c* being the standard deviation of ln(*x*). The *b* and *c* values can be directly used to compare with other specimens. Here, only one asphalt mixture specimen was scanned, requiring a lot of follow-up work to verify the effectiveness of this method.

Summary and Conclusion

A series of work for component segmentation, adhesive particle separation, contacting particle judgment, effective contact pixel searching, and statistical analysis of input data were developed to analyze the contact status of aggregates on asphalt mixture in a non-destructive way by using X-ray computed tomography images.

From the 2D images, the positional relationship of different particles can be clearly observed. Digital image processing methods are very important in getting high quality images, and the process can separate the aggregates from the complex asphalt mixture successfully with a series of procedures. The contact searching method can describe the contact degree of a single particle with different surrounding particles in a digital way, by which "contact searching pixels" data can be recorded and analyzed easily.

It will be statistically significant to use all 2D slice images together for analysis instead of a single section. Through careful data analysis, how the contact status changes along with different depths of the specimen and how the main contact form changes according to the pixel frequency histogram shape can be known. Three alternative quantitative indicators, *C*1, *C*2, and *C*3, were established and tested, and 4 different PDFs (Normal distribution, Lognormal distribution, Gamma distribution, and Weibull distribution) were fitted to the input data of *C*1, *C*2, and *C*3. After a series of statistical analyses, *C*1 was considered to be the most appropriate indicator that can assess the stone-stone contact degree in a non-destructive way.

The traditional VCA method is considered manual work, so there is the possibility of human error. Moreover, the volume parameters can only be acquired directly by bulk relative density measurement, and the density measurement process has its shortcomings which can't be avoided. The new method implements a totally digital way, by which human errors will not appear. We can now not only know the contact status along with the asphalt mixture specimen's depth but also easily compare the contact degree from specimen to specimen by statistical analysis. Thus, the new method is a useful approach to quantify the contact degree between aggregates in the asphalt mixtures.

Future Work

Future work will focus on testing different asphalt mixtures to see whether this indicator can apply to all kinds of cases. The data,

especially the mean value and the standard deviation value, will be compared with each other to judge whether this method can effectively distinguish the different contact degree of different asphalt mixtures and different compaction method. Moreover, the data will be analyzed carefully before and after loading to explore the indicator value changing rule.

In addition, future work will attempt to improve the search algorithm from 2D to 3D based on the sequence of images. Thus, the relative position of coarse aggregate particles in three-dimensional space can be evaluated directly, and related work and results will be subsequently reported.

Acknowledgements

Support is greatly acknowledged from the Key Project of National Natural Science Foundation of China (NSFC) under Grant No. 51038004 and the Western China Communications Construction and Technology Project under Grant No. 2009318000078.

References

1. Zhang, X.N., Wang, S.H., and Wu K.H. (2001). CAVF Method of Asphalt Mixture Design, *Highway*, 2(12), pp. 17-20 (in Chinese).
2. Xu, K., Zhang, X.N., and Wang D.Y. (2005). A Measurement Method of Percent Voids in Coarse Mineral Aggregates in Asphalt Mixtures Based on Digital Image Processing Technique, *Highway*, 11(11), pp. 151-154 (in Chinese).
3. You, Z.P., Adhikari, S., and Kutay, M.E. (2009). Dynamic Modulus Simulation of the Asphalt Concrete Using the X-ray Computed Tomography Images, *Materials and Structures*, 42(5), pp. 617-630.
4. Wang, L.B., Paul, H.S., Harman, T., and Angelo, J.D. (2004). Characterization of Aggregates and Asphalt Concrete Using X-ray Computerized Tomography: A State of the Art Report, *Journal of the Association of Asphalt Paving Technologists*, Vol. 73, pp. 467-500.
5. Masad, E., Arambula, E., Ketcham, R., Abbas, A., and Martin, A.E., (2007). Nondestructive Measurements of Moisture Transport in Asphalt Mixtures, *Journal of the Association of Asphalt Paving Technologists*, Vol. 76, pp. 919-952.
6. Masad, E. (2004). X-ray Computed Tomography of Aggregates and Asphalt Mixes, *Materials Evaluation*, 62(7), pp. 775-783.
7. Wang, L.B., Wang, X., Mohammad, L.N., and Wang, Y.P. (2004). Application of Mixture Theory in the Evaluation of Mechanical Properties of Asphalt Concrete, *Journal of Materials in Civil Engineering*, 16(2), pp. 167-174.
8. Masad, E., Jandhyala, V.K., and Dasgupta, J. (2002). Characterization of Air Void Distribution in Asphalt Mixes Using X-ray Computed Tomography, *Journal of Materials in Civil Engineering*, 14(2), pp. 122-129.
9. Yu, J.M., Li, X.J., Wang, D.Y., and Zhang, X.N. (2006). Finite Element Modeling of Asphalt Mix with X-ray Computerized Tomography Processing, *Journal of South China University of Technology: Nature Science Edition*, 26(1), pp. 16-19.
10. Masad, E., Castelblanco, A., and Birgisson, B. (2006). Effects of Air Void Size Distribution, Pore Pressure, and Bond Energy on Moisture Damage, *Journal of Testing and Evaluation*, 34(1), pp. 15-23.
11. Wang, L.B., Frost, J.D., Voyiadjis, G.Z., and Harman, T.P. (2003). Quantification of Damage Parameters Using X-ray Tomography Images, *Mechanics of Materials*, 35(8), pp. 777-790.
12. Masad, E. and Button, J. (2004). Implications of Experimental Measurements and Analyses of the Internal Structure of HMA, *Transportation Research Record*, No. 1891, pp. 212-220.
13. Garboczi, E.J. (2002). Three-dimensional Mathematical Analysis of Particle Shape Using X-ray Tomography and Spherical Harmonics: Application to Aggregates Used in Concrete, *Cement and Concrete Research,* 32(10), pp. 1621–1638.
14. Erdogan, S.T., Quiroga, P.N., Fowler, D.W., Saleh, H.A., Livingston, R.A., Garboczi, E.J., Ketcham, P.M., Hagedorn, J.G., and Satterfield, S.G. (2006). Three Dimensional Shape Analysis of Coarse Aggregates: Methodology and Preliminary Results on Several Different Coarse Aggregates, *Cement and Concrete Research,* 36(9), pp. 1619-1627.
15. Taylor, M.A., Garboczi, E.J., Erdogan, S.T., and Fowler, D.W. (2006). Some Properties of Irregular Particles in 3-D, *Powder Technology*, 162, pp. 1–15.
16. Wang, L.B., Frost, J.D., and Lai, J.S. (2004). Three Dimensional Digital Representation of Granular Material Microstructure from X-ray Tomography Imaging, *Journal of Computing in Civil Engineering*, ASCE, 18 (1), pp. 28–35.
17. Masad, E., Saadeh, S., Al-Rousan, T., Garboczi, E., and Little, D. (2005). Computations of Particle Surface Characteristics Using Optical and X-ray CT Images, *Computational Materials Science*, 34, pp. 406–424.
18. Sun, Z.Y., Sha, A.M., and Yao, Q.L. (2005). Realization of Threshold Segmentation Algorithm in Asphalt Mixture, *Journal of Chang'an University (Natural Science Edition)*, 25(6), pp. 34 -38 (in Chinese).
19. Schmitt, O., and Hasse, M. (2008). Morphological Multiscale Decomposition of Connected Regions with Emphasis on Cell Clusters, *Computer Vision and Image Understanding*, 113, pp. 188–201.
20. Elseifi, M.A., Al-Qadi, I.L., Yang, S.H., and Carpenter, S.H. (2008). Validity of Asphalt Binder Film Thickness Concept in Hot-Mix Asphalt, *Paper No. 08-0603*, Transportation Research Record: Journal of the Transportation Research Board, Vol. 2057, pp.37-45.
21. Graham, L.D., Smith, S.D., and Dunlop, P. (2005). Lognormal Distribution Provides an Optimum Representation of the Concrete Delivery and Placement Process, *Journal of Construction Engineering and Management*, 131(2), pp. 230-238.
22. Montgomery, D.C. and Runger, G.C.,(1994). *Applied Statistics and Probability for Engineers*, Wiley, New York, USA.
23. Kottegoda, N. T. and Rosso, R. (1998). *Statistics, Probability, and Reliability for Civil and Environmental Engineers*, McGraw-Hill, Singapore.
24. Neville, A.M. and Kennedy, J.B. (1964). *Basic Statistical Methods for Engineers and Scientists*, International Textbook Co., Scranton, PA, USA.

25. Law, A.M. and Kelton, W.D. (1991). *Simulation Modeling and Analysis*, 2nd Ed., McGraw-Hill, New York, USA.
26. Abourizk, S.M., Halpin, D.W., and Wilson, J.R. (1991). Visual Interactive Fitting of Beta Distributions, *Journal of Construction Engineering and Management,* 117(4), pp. 589–605.
27. Abourizk, S.M., Halpin, D.W., and Wilson, J.R. (1994). Fitting Beta Distributions Based on Sample Data, *Journal of the Construction Division*, 120(2), pp. 288–305.
28. Clemmens, J.P. and Willenbrock, J.H. (1978). The SCRAPESIM Computer Simulation, *Journal of Construction Engineering and Management*, 104(4), pp. 419–435.